PARAMETRIC OPTIMIZATION OF A FLEXURE-BASED ACTIVE GURNEY FLAP MECHANISM FOR MINIMUM STRESS

Jon Freire Gómez[a,*], Julian D. Booker[a], Phil H. Mellor[b]

[a] Dept. of Mechanical Engineering, University of Bristol, Queen's Building, University Walk, Bristol, BS8 1TR, UK

[b] Dept. of Electrical and Electronic Engineering, University of Bristol, Merchant Venturers Building, Woodland Road, Bristol, BS8 1UB, UK

Abstract

The EU's Green Rotorcraft programme is pursuing the development of a functional and airworthy Active Gurney Flap (AGF) for a full-scale helicopter rotor blade. Interest in the development of this 'smart adaptive rotor blade' technology lies in its potential to provide a number of aerodynamic benefits, which would in turn translate into a reduction in fuel consumption and noise levels. The AGF concept under development was selected following a design methodology presented in a previous publication and is characterized by the employment of crossed flexure pivots, which provide important advantages over bearings as they are not susceptible to seizing and do not require any maintenance (i.e. lubrication or cleaning). A baseline design of said mechanism was successfully tested both in a fatigue rig and in a 2D wind tunnel environment at flight-representative deployment schedules. However, finite element analysis of the baseline design under full in-flight centrifugal accelerations, aerodynamic loads and blade deformations shows that the stresses arising on the flexures would compromise their mechanical integrity. This paper investigates the potential to reduce the stresses on the flexures through parametric optimization of the baseline design. To this end, a procedure combining a simplified finite element model of the mechanism and an optimization algorithm is employed. From all the parameters required to fully define the mechanism, only those deemed to be the most influential were taken as optimization variables. The optimization approach adopted manages to reduce the stress on all flexures to levels below the yield stress, yet not enough so as to fulfil the design requirements in terms of safety margin and fatigue life. Future work will assess the scope for further stress reduction by altering additional design parameters.

1. INTRODUCTION

The performance of a helicopter is, to a great extent, determined by the aerodynamic behaviour of its main rotor. With the advent of computational fluid dynamics (CFD), helicopter blades have undergone an important shape optimization process, to the point of having virtually exhausted the scope for further aerodynamic improvement through changes in their geometry. At this stage, additional performance enhancement calls for morphing blades, i.e. smart adaptive structures capable of altering their shape while in service. In this context, the Green Rotorcraft [1] programme —which is part of the European Clean Sky Joint Technology Initiative (JTI)—, is pursuing the development of an Active Gurney Flap (AGF) for a full-scale helicopter rotor blade. Interest in the development of this 'smart adaptive rotor blade' technology lies in its potential to provide a number of aerodynamic benefits, which would in turn translate into a reduction in fuel consumption and noise levels.

The AGF concept under development was selected following a design methodology presented in a previous publication [2]. One of the main strengths of the chosen concept lies in the employment of crossed flexure pivots in lieu of bearings. These provide a number of important advantages over conventional joints as they are easily customisable, lightweight, maintenance free, backlash free (thus allowing precise control of position), they do not suffer from frictional losses and they eliminate the possibility of a jam during motion [3,4].

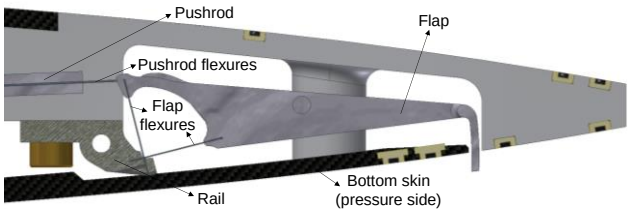

Fig. 1 Detail of the baseline AGF mechanism around the trailing edge region showing the crossed flexure pivots.

* Corresponding author. Tel.: +44 (0) 117 331 5460.
E-mail address: Jon.Freire@bristol.ac.uk (J. Freire Gómez).

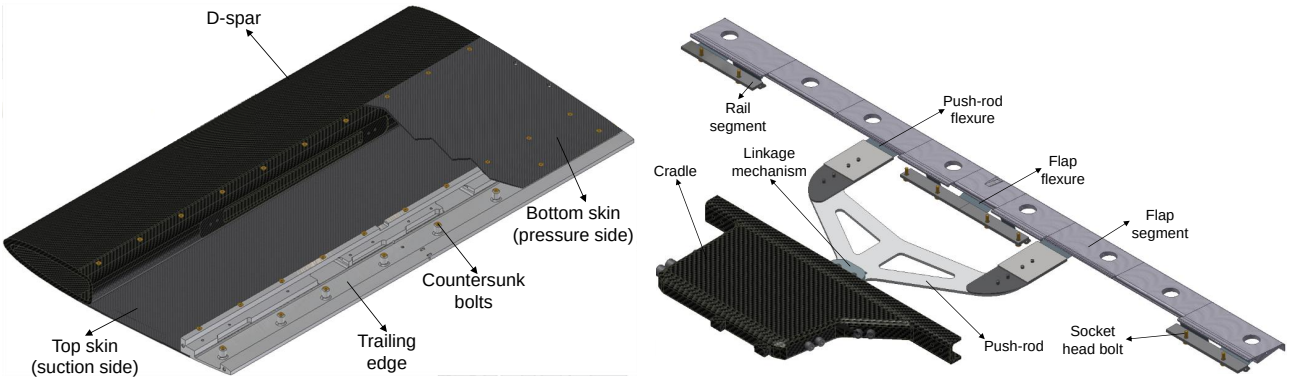

Fig. 2 Left: Interrupted view of the modified NACA 0012 aerofoil section with the baseline AGF mechanism removed; Right: Isometric view of the baseline AGF mechanism with a 900mm long flap.

Said AGF concept consists essentially of: a cradle slotted in the D-spar of the blade which houses an actuator and a linkage/gearing mechanism; a push-rod that transfers the movement from the leading edge to the trailing edge; and a flap hinging on leaf-spring crossed flexure pivots which are, in turn, anchored to the blade structure.

A baseline design of said AGF concept (see Figs. 1 and 2) was successfully tested both in a fatigue rig and in a 2D wind tunnel environment at flight-representative deployment schedules (see references [5,6] for more details). The system was designed to fit into a NACA 0012 aerofoil with a thickened trailing edge (3% chord thickness at 95% chord), with the flap sitting at 95% chord (chord=508mm).

After this successful stepping stone towards full validation of the AGF concept, the above design is currently being reengineered with a view to making it fit for flight test. A schematic of the baseline AGF design in its flight test version, with two independent 500mm long AGFs (see Fig. 4) centred at 60% rotor radius is shown in Fig. 3. However, finite element analysis of this baseline design under full in-flight loads and blade deformations (see Table 2) indicates that the stresses arising in the flexures would exceed the ultimate stress of the leaf-springs' material (stainless steel 17-7 PH in condition TH1050 with σ_u=1375MPa [7,8]) therefore causing them to break (see Table 4 and Fig. 8). Consequently, before the concept can be safely taken to flight test, design changes geared at reducing the maximum stress in the leaf-springs are needed.

To this end, two complementary approaches were decided to be investigated. The first approach consisted in focusing on the crossed flexure pivots as isolated entities and in trying to reduce the stress resulting from their pivotal rotation through shape optimization of their leaf-springs (see references [9,10]). The second approach, which is addressed in the present paper, investigates the potential for stress reduction through parametric optimization of the baseline mechanism as a whole, while sticking to constant cross section leaf-springs. The methodology employed to tackle the analysis is covered in Section 2, while the results are presented in Section 3. The main conclusions are outlined in Section 4.

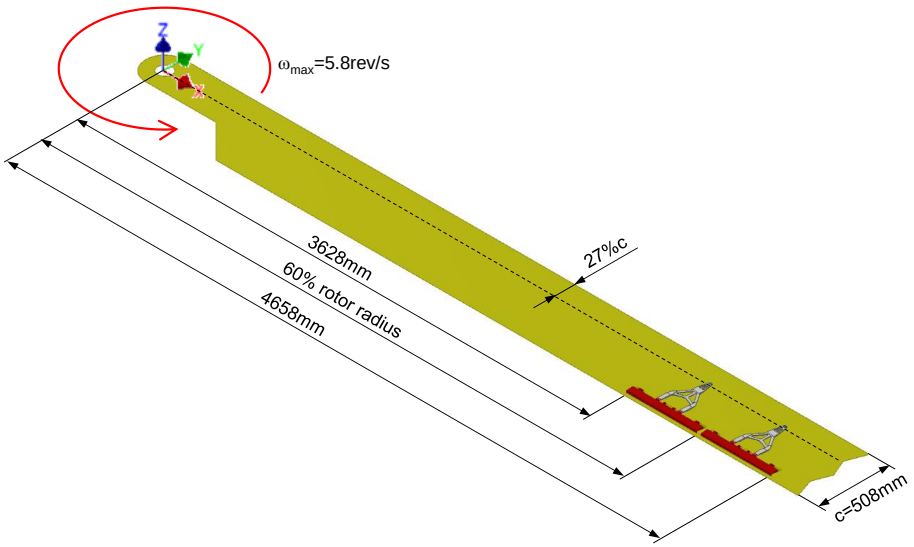

Fig. 3 Schematic showing two independent 500mm long AGFs centred at 60% rotor radius.

2. METHODOLOGY

2.1. Modelling assumptions and analysis method

As mentioned in the previous section, the baseline design consists of two identical and independent 500mm long AGFs centred at 60% rotor radius. Each flap —assumed to be manufactured in titanium and with a mass conservatively estimated at 250g based on preliminary CAD drawings— is linked to the blade structure via seven crossed flexure pivot leaf-springs, all with an active length of 10.14mm. Each pushrod —assumed to be manufactured in aluminium and with a conservative mass estimate of 150g— is attached to its corresponding flap via two flexures, both with an active length of 9.4mm (see row labelled 'ref.' in Table 4 and Fig. 8 for the spanwise position, as well as the width and thickness dimensions of all flexures in the 'reference' baseline design).

The fact that both AGFs are assumed to be geometrically equal simplifies things and allows the analysis to be restricted to the outboard AGF, which is the one subjected to the most severe loading and blade deflections. The rationale behind this is that if the optimization proves there is scope to reduce stress on the outboard AGF enough so as to make the concept fit for flight, there will be even greater scope to do so on the less severely loaded inboard AGF.

With regard to the actuator and the gearing/linkage mechanism, these need not be included in the analysis as their effect can be replaced by a linear stroke input applied directly on the forward end of the pushrod. Another interesting aspect that should be pointed out is that, in the mechanism's undeformed state, the flap is half deployed in order to minimise the angular deflection of the leaf-springs between the full deployment and full retraction positions (see Fig. 1 and reference [5]).

Considering the crossed flexure pivots featured in the design are much more flexible than the rest of the components (namely the flap and the pushrod) and further taking into account that the leaf-springs in the pivots are prismatic-type members, it was deemed appropriate to discretize the AGF mechanism into a parameterized 3D model of interconnected Timoshenko-type [11] beam elements (see Fig. 4). Those elements representing the leaf-springs (i.e. elements 15, 17, 19, 21, 23, 25, 27, 29 and 31) were modelled as flexible and were assigned a Young's modulus of E=200GPa and a density of ρ=7640kg/m^3 (see physical and mechanical properties corresponding to stainless steel 17-7 PH in [7,8]). Conversely, the elements representing the pushrod (namely numbers 32, 33, 34 and 35) and the flap (the remainder) were modelled as perfectly rigid and were assigned a Young's modulus of E=10^{10}GPa. The flap elements were assigned a variable density —updated in each iteration of the optimization process— such that the sum of their individual masses would permanently yield a total flap mass of 250g. Similarly, the density assigned to the pushrod elements was also updated on each iteration with the target of keeping the total pushrod mass at 150g. The need to update the aforementioned densities on each iteration arises as the result of the effect that the design parameters taken as optimization variables have on the lengths of some of the flap and pushrod elements, and by extension, on the total flap and pushrod masses.

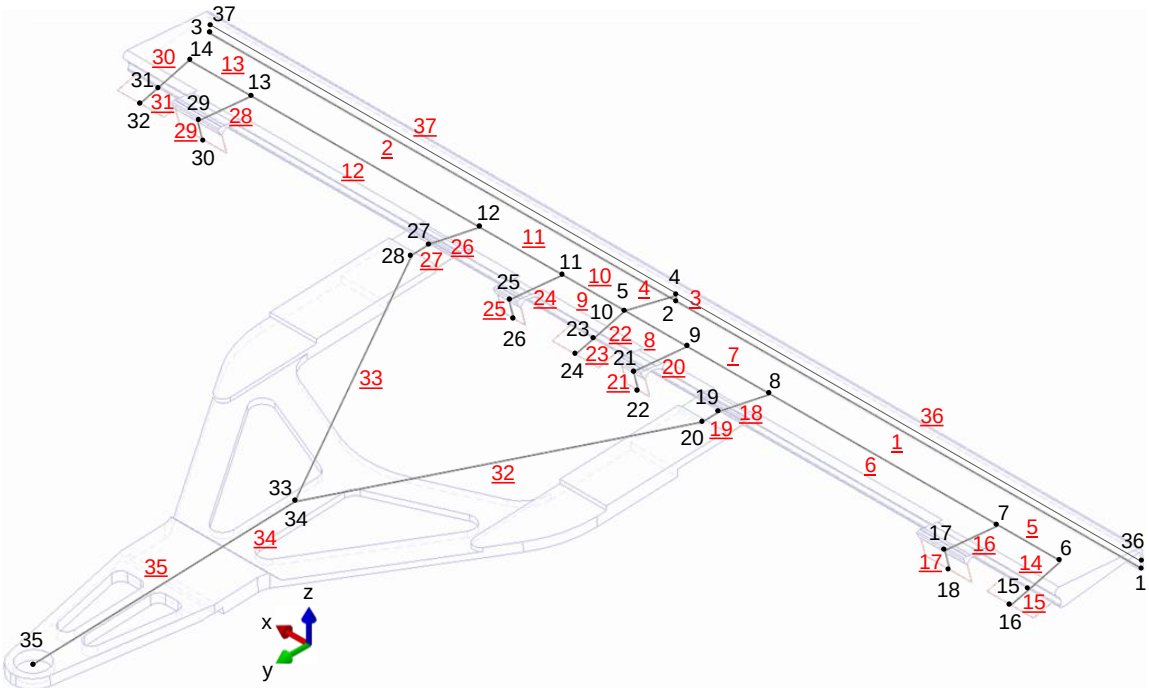

Fig. 4 Discretized FE model of the baseline AGF mechanism as shown in Fig. 3.

The structural performance of the above model can be characterized through matrix equation {F}=[K]{u}, where {F} is the vector of nodal forces, {u} is the vector of nodal displacements and [K] is the global stiffness matrix of the system, which can be obtained by appropriately assembling the local stiffness matrices (defined in [12]) of all individual beam elements. Said matrix equation can be solved using the Direct Stiffness Method [12], which is a particularization of the Finite Element Method (FEM) that enables the specific in-flight loading and blade deflection conditions to be readily applied on the model (see Fig. 7).

It should be noted that the above equation corresponds to a quasi-static type of analysis, which yields accurate results only if the highest frequency of the loading acting on the system is —as a rule of thumb— at least four times lower than the fundamental frequency of the system itself. In the case of the AGF mechanism, the highest excitation frequency comes, not from the blade, but from the deployment/retraction movement of the mechanism, whose maximum operational frequency is approximately 30Hz. Therefore, for a quasi-static type of analysis to be acceptable the fundamental frequency 'ω_n' of the AGF design should be at least $\omega_n \geq 120$Hz. In order to verify this requirement, the fundamental frequency of the model (which was estimated at 314Hz for the original baseline design) was calculated on each iteration of the optimization process by solving the equation $|[K]-\omega^2[M]|=0$, where [K] is again the global stiffness matrix of the system, 'ω' any one of its natural frequencies and [M] the global mass matrix of the system which can be obtained by appropriately assembling the local mass matrices (also defined in [12]) of all individual beam elements.

As regards the boundary conditions employed, the model is assumed to be fixed (to the blade) at nodes 16, 18, 22, 24, 26, 30, and 32. Bearing in mind that the blade has a much greater mass and stiffness than the AGFs within it, the deformations suffered by the former are assumed to be unaffected by the presence of the latter. Accordingly, the deflections pertaining to a naked blade case were used for the analysis. In the corresponding load cases (see Section 2.2), these deflections were applied directly on the aforementioned nodes in the form of known displacements. Finally, node 35 —which represents the connection point to the linkage/gearing mechanism— was modelled as a fixed spherical joint, thus allowing node 35 to freely rotate. In those loading cases where a full flap deployment/retraction was required (see Section 2.2), the necessary pushrod movement was simulated by applying a known displacement directly on node 35 in the axial direction of element 35.

Once the vector of nodal displacements {u} is obtained from the equation above, this can be used, together with the individual stiffness matrix of each leaf-spring element, to calculate the forces acting at their ends (see Fig. 5). In turn, these forces will be used to calculate the stresses at any point throughout the leaf-springs. For the purposes of this study, in each leaf-spring stress was only evaluated at the 99 points shown in Fig. 5. The generic stress state at any one of them (shown on the top right-hand side of Fig. 5) can be mathematically described through the symmetrical stress tensor shown in Eq. (1):

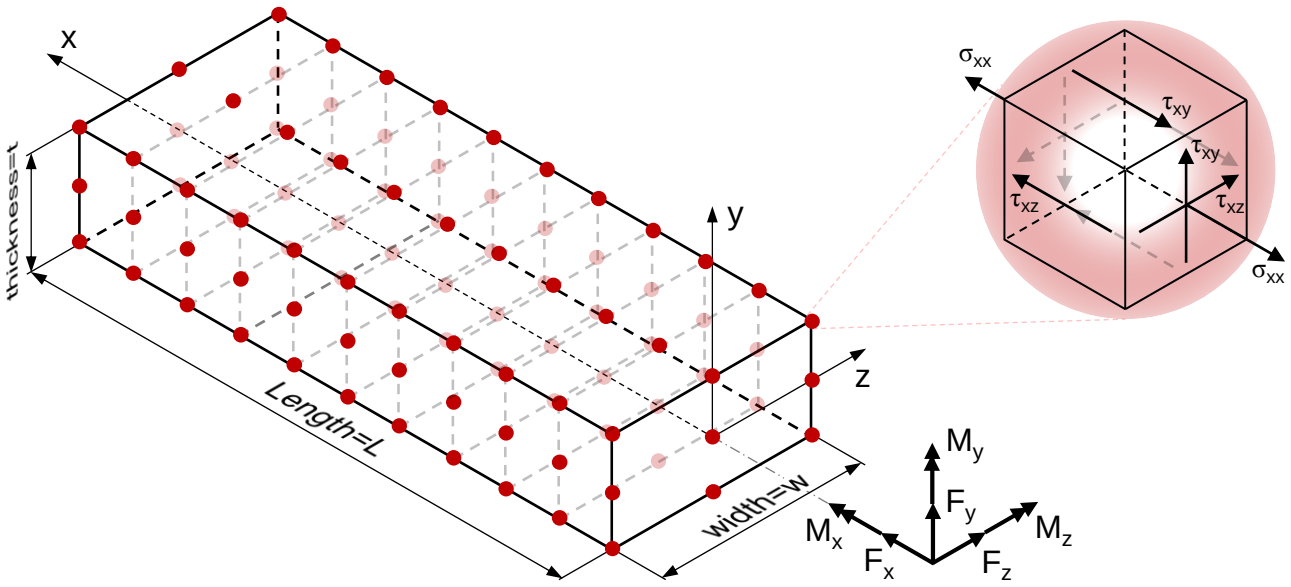

Fig. 5 Generic leaf-spring in equilibrium (left) subjected to loads F_x, F_y, F_z, M_x, M_y and M_z at one of its ends. The 99 red dots on the leaf-spring represent the points at which stress is evaluated. The generic stress state arising in each one of them is shown on the top right hand side.

$$(1)\qquad [\sigma]=\begin{bmatrix}\sigma_{xx} & \tau_{yx} & \tau_{zx}\\ \tau_{xy} & \sigma_{yy} & \tau_{zy}\\ \tau_{xz} & \tau_{yz} & \sigma_{zz}\end{bmatrix}=\begin{bmatrix}\sigma_{xx} & \tau_{xy} & \tau_{xz}\\ \tau_{xy} & 0 & 0\\ \tau_{xz} & 0 & 0\end{bmatrix}$$

Where σ_{xx}, τ_{xy} and τ_{xz} can be calculated as [12,13]:

$$(2)\qquad \sigma_{xx}=\sigma_{F_x(x)}+\sigma_{M_y(x)}+\sigma_{M_z(x)}=\frac{-F_x}{t_i w_i}-\frac{(M_y+xF_z)z}{\frac{1}{12}t_i w_i^3}+\frac{(M_z-xF_y)y}{\frac{1}{12}w_i t_i^3}\quad \forall\, i\in\{15,17,19,21,23,25,27,29,31\}$$

$$(3)\qquad \tau_{xy}=\frac{3F_y}{2t_i w_i}\left[1-\left(\frac{y}{\frac{t_i}{2}}\right)^2\right]+\underbrace{\frac{-z}{\frac{w_i}{2}}\eta\frac{M_x}{\alpha w_i t_i^2}}_{N.B.:\ only\ at\ points\ \left(x,0,\pm\frac{w_i}{2}\right)}\quad \forall\, i\in\{15,17,19,21,23,25,27,29,31\}$$

$$(4)\qquad \tau_{xz}=\frac{3F_z}{2t_i w_i}\left[1-\left(\frac{z}{\frac{w_i}{2}}\right)^2\right]+\underbrace{\frac{y}{\frac{t_i}{2}}\frac{M_x}{\alpha w_i t_i^2}}_{N.B.:\ only\ at\ points\ \left(x,\pm\frac{t_i}{2},0\right)}\quad \forall\, i\in\{15,17,19,21,23,25,27,29,31\}$$

The values for α and η are given in Table 1.

Table 1 Values for the α and η parameters as a function of the beam's w/t ratio [13].

w_i/t_i	1.0	1.5	2.0	3.0	6.0	10.0	∞
α	0.208	0.231	0.246	0.267	0.299	0.313	0.333
η	1.000	0.859	0.795	0.753	0.743	0.742	0.742

Finally, the Von Misses stress at any point in the leaf-spring can be calculated according to Eqs. (5)-(7), where σ_1, σ_2 and σ_3 are the principal stresses at the point in question:

$$(5)\qquad |[\sigma]-\lambda[I]|=0\quad\Rightarrow\quad\begin{vmatrix}\sigma_{xx}-\lambda & \tau_{xy} & \tau_{xz}\\ \tau_{xy} & -\lambda & 0\\ \tau_{xz} & 0 & -\lambda\end{vmatrix}=0\quad\Rightarrow$$

$$\lambda\cdot\left[-\lambda^2+\sigma_{xx}\cdot\lambda+\left(\tau_{xy}^2+\tau_{xz}^2\right)\right]=0$$

$$(6)\qquad \begin{cases}\sigma_1=\lambda_1=\frac{\sigma_{xx}}{2}+\sqrt{\left(\frac{\sigma_{xx}}{2}\right)^2+\left(\tau_{xy}^2+\tau_{xz}^2\right)};\\ \sigma_2=\lambda_2=\frac{\sigma_{xx}}{2}-\sqrt{\left(\frac{\sigma_{xx}}{2}\right)^2+\left(\tau_{xy}^2+\tau_{xz}^2\right)};\\ \sigma_3=\lambda_3=0;\end{cases}$$

$$(7)\qquad \sigma_{VM}=\sqrt{\sigma_1^2+\sigma_2^2-\sigma_1\sigma_2}$$

2.2. Loading and blade deflections

The loads and blade deflections used for the analysis are shown in Table 2, where they have been grouped into different sets depending on whether or not they occur simultaneously. It is worth reminding that, on the grounds explained in Section 2.1, these loads and deflections correspond with those the outboard AGF is subjected to.

Set A encompasses the loads and deflections which are constantly present throughout the time the helicopter is airborne. This set includes: the gravitational and centrifugal loads acting on the flap and the pushrod (which are applied at their respective centres of mass, namely nodes 5 and 34 in Fig. 4), and the axial extension experienced by the blade over the AGF region (applied on nodes 16, 18, 22, 24, 26, 30, 32 and 35 as a known displacement given by Eq. (8), where EA and F_{radial} can be found in Table 3, and d_i are described in Fig. 8). The values of the centrifugal loads were calculated considering a rotor speed of 5.8rev/s and 5rev/s for the 'limit' and 'normal operation' cases respectively. In the case of the axial extensions, a reduction factor of 0.7 was applied to Eq. (8) for the 'normal operation' case.

Table 2 Loads and deflections acting on the outboard AGF shown in Fig. 3.

			LIMIT CASE						NORMAL OPERATION					
			x	y		z			x	y		z		
A	Flap weight	[N]	-	-		-2.45			-	-		-2.45		
	Pushrod weight	[N]	-	-		-1.47			-	-		-1.47		
	Centrifugal force on flap	[N]	1464	-108		-			1088	-81		-		
	Centrifugal force on pushrod	[N]	879	-35		-			653	-27		-		
	Radial extension of blade (Δx_{max})	[mm]	0.56	-		-			0.39	-		-		
B	Aerodynamic loads (distributed)	[N]	-	0	-288	0	-42		-	0	-288	0	-42	
	Pushrod travel (p) for flap retraction/deployment	[mm]	-	p·cos(2.36)		-p·sin(2.36)			-	p·cos(2.36)		-p·sin(2.36)		
C	Flap chordwise inertia	[N]	-	95	0	-80	-		-	18	0	-30	-	
	Pushrod chordwise inertia	[N]	-	57	0	-48	-		-	11	0	-18	-	
D	Flap out-of-plane inertia	[N]	-	-		242	0	-310	-	-		102	0	-190
	Pushrod out-of plane inertia	[N]	-	-		145	0	-186	-	-		61	0	-114
E	Blade lag (Δy_{max})	[mm]	-	0.21	0	-0.21	-		-	0.12	0	-0.12	-	
F	Blade flap (Δz_{max})	[mm]	-	-		2.24	0	-2.24	-	-		1.34	0	-1.34
G	Blade twist (θx_{max})	[deg]	0.16	0	-0.16	-			0.16	0	-0.16	-		

(8)
$$\Delta x = \frac{d_i}{L}\Delta x_{max} = \frac{d_i}{L}\frac{L}{EA}F_{radial} = \frac{d_i}{EA}F_{radial}$$
$$\forall\ i \in \{15,17,19,21,23,25,27,29,31\}$$

Set B groups the loads associated with the full deployment/retraction states of the flap. These include the chordwise and out-of-plane aerodynamic loads present at full deployment (applied as distributed loads on elements 36-37 and 1-2 respectively), and the pushrod displacement 'p' (applied on node 35 in the axial direction of element 35) required to guarantee either a full retraction or a minimum deployment of 1% chord (i.e. 5mm) of all points along the flap's span.

Sets C and D consist of inertia loads produced by in-flight blade vibrations of random nature. These inertia loads acting on the flap and the pushrod are applied at their respective centres of mass, namely nodes 5 and 34. The aforementioned blade vibrations also cause blade deflections which are transmitted to the AGF mechanism (sets E to G). The flap, lag and twist deflections of the blade (shown in Fig. 7) affect nodes 16, 18, 22, 24, 26, 30, 32 and 35 making them not only displace but also rotate. In the 'limit' case, the displacements and deflections corresponding to each of the aforementioned nodes are given by Eqs. (10)-(13). For the 'normal operation' case, reduction factors of 0.6 (to M_{flap} and M_{lag}) and of 0.7 (to F_{radial}) were applied in said equations.

(9)
$$\theta_x = \frac{d_i}{L}\frac{\pi}{180}\theta_{x_{max}}$$
$$\forall\ i \in \{15,17,19,21,23,25,27,29,31\}$$

(10)
$$\theta_y = arcsin\left(\frac{\frac{d_i}{L}2R_{flap}\sin\theta_{y_{max}} - R_{flap}\sin\theta_{y_{max}}}{R_{flap}}\right) =$$
$$= arcsin\left[\left(2\frac{d_i}{L} - 1\right)\sin\theta_{y_{max}}\right]$$
$$\forall\ i \in \{15,17,19,21,23,25,27,29,31\}$$

(11)
$$\Delta z = R_{flap}\left(cos\theta_y - cos\theta_{y_{max}}\right) = \frac{EI_y}{M_{flap}}\left(cos\theta_y - cos\theta_{y_{max}}\right)$$

(12)
$$\theta_z = arcsin\left(\frac{R_{lag}\sin\theta_{z_{max}} - \frac{d_i}{L}2R_{lag}\sin\theta_{z_{max}}}{R_{lag}}\right) =$$
$$= arcsin\left[\left(1 - 2\frac{d_i}{L}\right)\sin\theta_{z_{max}}\right]$$
$$\forall\ i \in \{15,17,19,21,23,25,27,29,31\}$$

(13)
$$\Delta y = R_{lag}\left(cos\theta_z - cos\theta_{z_{max}}\right) = \frac{EI_z}{M_{lag}}\left(cos\theta_z - cos\theta_{z_{max}}\right)$$

where EA, F_{radial}, EI_y, M_{flap}, EI_z, M_{lag}, can be found in Table 3, d_i are described in Fig. 8, and $\theta_{y_{max}}$ and $\theta_{z_{max}}$ are given by Eqs. (14)-(15).

(14)
$$\theta_{y_{max}} = \frac{\frac{L+\Delta x}{2}}{R_{flap}} = \frac{L\left(1+\frac{F_{radial}}{EA}\right)}{2\frac{EI_y}{M_{flap}}}$$

(15)
$$\theta_{z_{max}} = \frac{\frac{L+\Delta x}{2}}{R_{lag}} = \frac{L\left(1+\frac{F_{radial}}{EA}\right)}{2\frac{EI_z}{M_{lag}}}$$

Table 3 Blade section constants in the region of the AGFs and limit loads acting on the blade.

RADIAL		FLAP		LAG	
EA	F_{radial}	EI_y	M_{flap}	EI_z	M_{lag}
[N]	[N]	[Nmm^2]	[Nm]	[Nmm^2]	[Nm]
2.1E+08	236427	9.E+10	6434	2.4E+12	15820

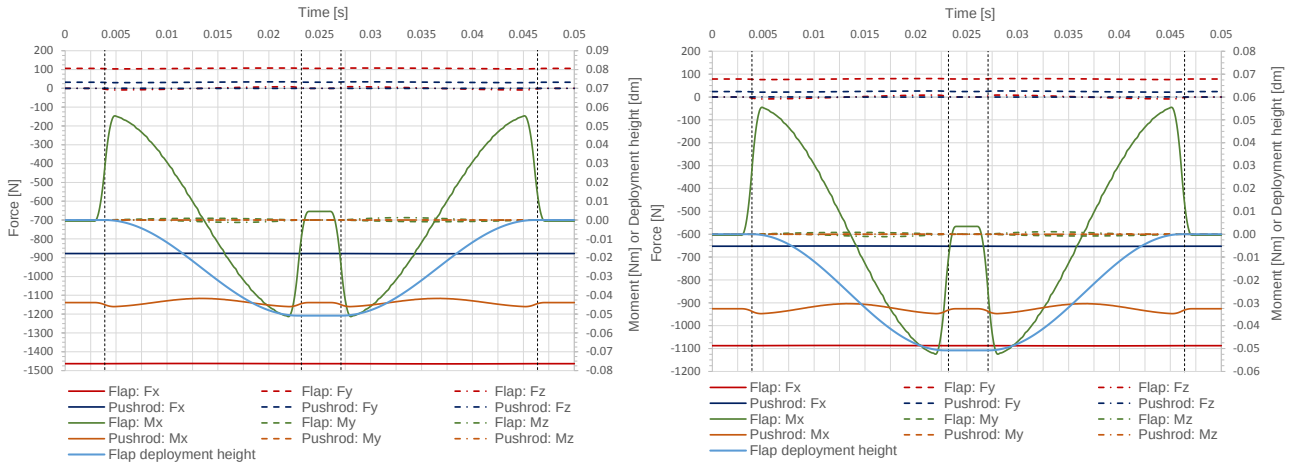

Fig. 6 Outboard flap and pushrod inertia loads corresponding to a 'deployment @ 26.3Hz - hold - retraction @ 26.3Hz' type of sequence (line in blue) for a rotor speed of 5.8rev/s ('limit' case, left) and 5rev/s ('normal operation' case, right).

With regard to the inertia loads associated with the deployment/retraction movement of the AGF mechanism, these were analysed using the multibody systems simulation tool 'Motion Simulation' integrated within Siemens' NX software [14]. The results of the analysis (displayed in Fig. 6) show that, with the exception of the centrifugal forces (already included in Set A), these loads are negligible and were therefore not considered in the analysis.

As can be observed in Table 2, loads and deflections in sets C to G may take three possible values: an upper bound value, a 'zero' value (if they are not present) or a lower bound value. Loads in set B may take two: either a given value or a 'zero' value. Whereas loads in set A can only take a single constant value as they are permanently present during the time the helicopter is airborne. This means that the AGF mechanism may be subjected to up to $1 \cdot 2 \cdot 3^5 = 486$ different load combinations during flight. As it is not possible to know which specific load combination will be the most severe (i.e. that giving rise to highest stress levels) beforehand, the mechanism will have to be analysed under each of the aforementioned load combinations. This does not mean, however, that equation [K]{u}={F} need be solved 486 times. Instead, by virtue of the principle of superposition applicable to linear equations such as the one concerned, it will be sufficient (and computationally much more cost-effective) to solve said equation 8 times and then to appropriately combine the displacement vectors {u} corresponding to each solution to obtain the individual responses of the 486 possible load combinations. Specifically, the 8 'basic' load cases that it will be sufficient to solve the above equation for are: the load case labelled set A; load cases C, D, E, F and G using either their upper bound values or their lower bound values; the 'aerodynamic loads' case within set B; and the 'pushrod travel 'p' for flap retraction/deployment' case also within set B, using an arbitrary reference value 'p_{ref}' for the pushrod travel. The reason why the two load cases within set B need to be analysed separately is that, depending on whether the flap is considered to be deployed or stowed, the amount of pushrod travel 'p' required to guarantee either a full retraction or a minimum deployment of 1% chord (i.e. 5mm) of all points along the flap's span in each of the 486 load combinations will be different. Hence the need to calculate the isolated response of the AGF model in terms of {u} under a pure 'pushrod travel' type of input.

2.3. Description of the optimization procedure

The analysis of the model presented in Section 2.1 and its optimization were carried out using Matlab [15]. The implementation of the Direct Stiffness Method written for this purpose was thoroughly tested using a model equivalent to that in Fig. 4 built in Abaqus [16]. Once the correctness of both the analysis method and the model was verified, these were coupled to an optimization algorithm (pattern search [15]) built into Matlab itself.

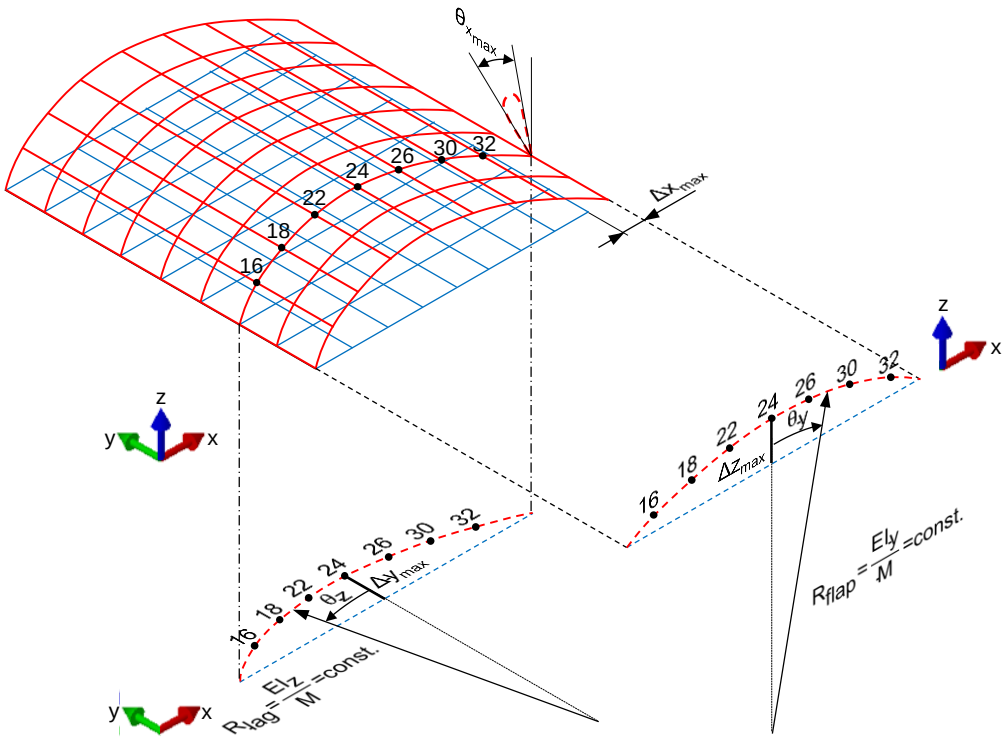

Fig. 7 Blade deflections transmitted to the AGF mechanism. Δz_{max} and Δy_{max} represent the flap and lag deflections respectively at the centre point of each 500mm long flap relative to a line joining the end points. The frame of reference and the node numbering are the same as those shown in Fig. 4.

The objective of the optimization was to minimize the stress in the flexures and to see whether this could be brought below the threshold of σ_y/SF=1300/1.5= 867MPa when subjecting the design to the limit loads. To this end, three different optimization runs were performed. In run I, from all the parameters required to fully define the mechanism, only the relative position of the flexures along the flap's span 'd_i' and their individual widths 'w_i' were taken as optimization variables (see Fig. 8). For run II, the central flexures joining the flap to the blade were removed from the model (namely elements 21, 23, and 25) and again the relative position of the remaining flexures along the flap's span 'd_i' and their individual widths 'w_i' were taken as optimization variables. For run III, in addition to those employed in run II, the flexure's individual thicknesses 't_i' were also taken as optimization variables. The results regarding the aforementioned optimization runs are discussed in Section 3.

In order to determine the highest possible stress, in each optimization iteration the model was analysed under the 486 different load combinations discussed in Section 2.2. It is important to note that each load combination requires a different amount of pushrod travel 'p' in order to guarantee —depending on the flap position corresponding to each load combination— either a full retraction or a full deployment (minimum of 1% chord, i.e. ~5mm) of the flap along its entire span. If both the flap and the blade remained perfectly straight under any loading condition, in order to calculate the required pushrod travel 'p' it would be sufficient to analyse the z-wise displacement of nodes 1 and 3 (i.e. the ends of the flap) under the load combination in question. However, since only the flap remains straight (being modelled as perfectly rigid), unlike the blade which is assumed to take the shape of a circular arc in flap, it will also be necessary to check the z-wise displacement of node 2 (i.e. the midpoint of the flap). To calculate the model's response under each load combination, firstly the pertinent individual responses corresponding to sets A, C-G and to the 'aerodynamic loads' case must be added together, thus obtaining a preliminary incomplete response (see reference to the principle of superposition in Section 2.2). In order to obtain the complete response of the system, it will be sufficient to add to the aforementioned incomplete response, the response corresponding to a reference pushrod travel 'p_{ref}' (which must have been separately calculated beforehand) multiplied by a factor such that nodes 1, 2 and 3 satisfy the corresponding deployment/ retraction requirement pointed out above. This factor must be calculated based on the z-wise displacement of whichever node (out of the aforementioned three) is furthest from fulfilling said deployment/retraction requirement according to the incomplete response.

As for the optimization constraints used in the optimization runs, the conditions/checks built into the algorithm were the following: a lower bound on the allowable width 'w_i' of the flexures of 1mm, the requirement for there to be a minimum distance between flexures of 0.5mm, for all flexures to fit completely within the flap's 500mm span, and for the fundamental frequency of the model to be always equal or greater than 120Hz as it evolves throughout the optimization process (see reasons explained in Section 2.1).

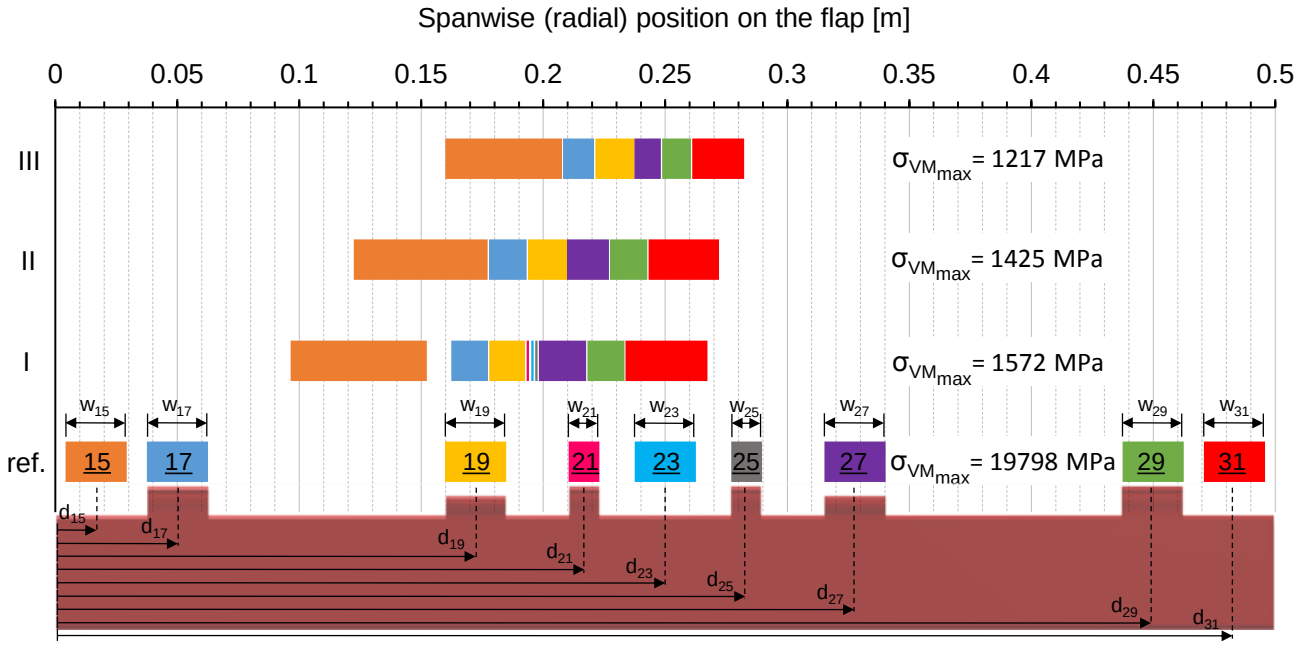

Fig. 8 Graphical presentation of the results in Table 4.

3. RESULTS

A graphical and a numerical representation of the optimization results is given in Fig. 8 and Table 4 respectively. Under the limit loads, the maximum stress arising in flexures of the baseline design (labelled as 'ref.' for 'reference design') was found to be 19798MPa, a value which is well above the yield strength of stainless steel 17-7-PH (σ_y=1300MPa). Consequently, in order to make the design viable and fit for flight, there was a clear need to reduce stress through optimization of the baseline mechanism.

Optimization I managed to bring the maximum stress arising in the flexures down to 1572MPa. This represents a significant reduction of 92.06% relative to the reference case, yet insufficient as said value remains above the material's yield strength. As can be observed in Fig. 8, said optimization tends towards a design where, in comparison to that of reference, the flexures are much closer to each other, distributed over a length of approximately 17cm, and centred about a point inboard relative to the flap's midpoint. A further interesting observation is that the resulting width for flexure elements 21, 23 and 25 is 1mm (i.e. the allowable minimum built into the optimization algorithm). This suggest that, had the width been kept completely unconstrained in the algorithm, these elements would have likely ended having a zero (or close to zero) width, which means that they are unimportant from a structural perspective and that it would likely be beneficial to have them completely removed from the design.

Based on this rationale, optimization run II was virtually a repetition of run I, the only difference being that the aforementioned elements were removed from the design and therefore left out of the optimization. In this second run II, the maximum stress was further reduced down to 1425MPa (see Table 4). This constitutes an important (yet still insufficient) reduction of 92.8% relative to the reference case. In light of these results and as a last resort to bring stress below the σ_y=1300MPa threshold, a third and last optimization run III was carried out where the flexure's individual thicknesses 't_i' were additionally taken as optimization variables. This final run III resulted in a maximum equivalent Von Mises stress of 1217MPa (i.e. a 93.85% reduction relative to the reference design). This result —which can be regarded as positive in as much as it provides a set of design parameter values such that the stress arising in the flexures is below the yield strength of their material— is, however, not quite the desirable as the design should also have a built-in safety margin for it to be considered airworthy. Consequently, the maximum stress should have been equal or less than σ_y/SF=1300/1.5=867MPa, considering a reasonable safety factor to be 1.5.

Despite the somewhat unsatisfactory result, bearing in mind that the limit loads used for the optimization are not representative of the predominant forces during flight, the design coming out of optimization run III was decided to be further analysed under the loads corresponding to the 'normal operation' case. The analysis shows that, even under this more benign loading scenario, the maximum stress arising in the flexures would still be above the target threshold of 867MPa(<895MPa). Therefore, as shown in Fig. 9, the design coming out of run III would not satisfy the viability requirements either from a safety margin perspective, or from a fatigue-life perspective (the flexures are required to have virtually infinite fatigue life and the endurance limit for stainless steel 17-7 PH is σ_e=510MPa).

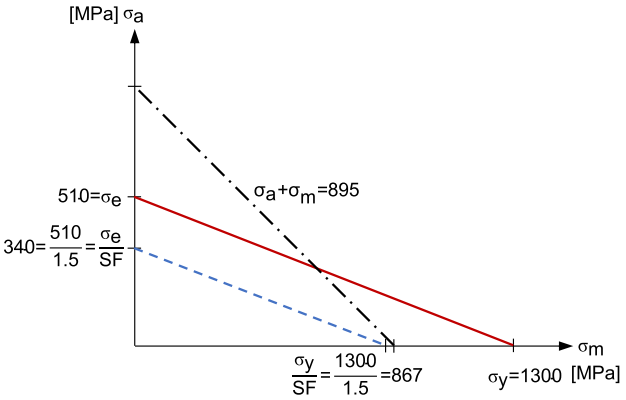

Fig. 9 Soderberg diagram corresponding to stainless steel 17-7 PH in condition TH 1050 in thin sheet form.

Table 4 Reference case compared with the results corresponding to optimization runs I, II, and III.

	σ_{VMmax}	σ ↓	fund. freq.	d_{15}	d_{17}	d_{19}	d_{21}	d_{23}	d_{25}	d_{27}	d_{29}	d_{31}	t_{15}	t_{17}	t_{19}	t_{21}	t_{23}	t_{25}	t_{27}	t_{29}	t_{31}	w_{15}	w_{17}	w_{19}	w_{21}	w_{23}	w_{25}	w_{27}	w_{29}	w_{31}
	[MPa]	[%]	[Hz]	[mm]	[mm]	[mm]	[mm]	[mm]	[mm]	[mm]	[mm]	[mm]	[μm]	[μm]	[μm]	[μm]	[μm]	[μm]	[μm]	[μm]	[μm]	[mm]	[mm]	[mm]	[mm]	[mm]	[mm]	[mm]	[mm]	[mm]
ref.	19798	0.00	314	16.7	50.0	172.2	216.7	250.0	283.3	327.8	450.0	483.3	(127)	(127)	(300)	(127)	(127)	(127)	(300)	(127)	(127)	25	25	25	12.5	25	12.5	25	25	25
I	1572	92.06	312	124.3	169.8	185.2	193.6	195.6	197.2	207.9	225.7	250.5	(127)	(127)	(300)	(127)	(127)	(127)	(300)	(127)	(127)	55.8	15.1	14.7	1.0	1.0	1.0	19.3	15.1	33.6
II	1425	92.80	317	149.8	185.4	201.7	-	-	-	218.3	235.0	257.6	(127)	(127)	(300)	-	-	-	(300)	(127)	(127)	54.8	15.5	16.1	-	-	-	17.1	15.3	28.9
III	1217	93.85	373	183.8	214.5	229.3	-	-	-	242.7	254.6	271.6	127	127	300	-	-	-	544	127	127	47.7	12.7	16.0	-	-	-	10.9	11.8	21.3

4. CONCLUSIONS

The optimization approach presented —consisting of coupling a simplified parameterized finite element model to an optimization algorithm— constitutes a useful and cost-effective method, especially well-suited to early design stages of complex mechanical systems difficult to handle otherwise. This method does obviously not guarantee a high accuracy in the stress predictions. However, it provides a good enough estimate so as to make a judgement on the viability of the design and to decide whether there is scope for it to be successfully put through a detail design phase.

When applied to the AGF mechanism under study, this optimization strategy yielded very significant stress reductions relative to the reference baseline design, namely bringing stress levels from 19798MPa down to 1217MPa (i.e. a reduction of 93.85%). However, despite the fact that the maximum stress of the optimized design is below the yield strength of the flexures' material, the stress reduction achieved is not sufficient as the equivalent safety margin is only 1.07 (it should be at least 1.5 for the design to be considered airworthy). It is important to point out that this result can be deemed to be somewhat pessimistic, as the modelling assumptions adopted were in some ways conservative (for instance, the flap and the pushrod were modelled as perfectly rigid when, actually, they have some compliance). Nevertheless, the impact of said assumptions on the results is believed to be small and in all probability these would not have changed greatly had more realistic assumptions been made. In view of this outcome, future work will look into altering additional design parameters to reduce stress even further.

ACKNOWLEDGEMENTS

This project is funded by the Clean Sky Joint Technology Initiative (JTI) (topic JTI-CS-2010-4-GRC-01-005), which is part of the European Union's 7th Framework Programme (FP7/2007-2013).

REFERENCES

[1] Clean Sky website - Green Rotorcraft - Blades (GRC1) - Techno streams, <http://www.cleansky.eu/content/page/innovative-rotor-blades-technology-streams> (29 April 2015).

[2] Freire Gómez J, Booker JD and Mellor PH. Design and development of an active Gurney flap for rotorcraft. *Proc. SPIE 8690*, San Diego (USA), 86900F, 2013.

[3] Howell LL, Magleby SP and Olsen BM. *Handbook of Compliant Mechanisms*. 1st edition, Wiley, 2013.

[4] Lobontiu N. *Compliant mechanisms: design of flexure hinges*. 1st edition, CRC Press, 2003.

[5] Loendersloot R, Freire Gómez J and Booker JD. Wind tunnel testing of a full scale helicopter blade section with an upstream active Gurney flap. *Proc. European Rotorcraft Forum*, Southampton (UK), 2014.

[6] Hoff SC van't, and Tuinstra M. Time-resolved stereo PIV measurements of an active Gurney flap system. *Proc. European Rotorcraft Forum*, Southampton (UK), 2014.

[7] *Department of Defense Handbook: Metallic materials and elements for aerospace vehicle structures (MIL-HDBK-5J)*, Department of Defense of the United States of America, 2003.

[8] Leybold HA. *Axial-load fatigue tests on 17-7 PH stainless steel under constant-amplitude loading. Technical Report TECHNICAL NOTE 0-439*. National Aeronautics and Space Administration (NASA), 1960.

[9] Freire Gómez J, Booker JD and Mellor PH. 2D shape optimization of leaf-type crossed flexure pivot springs for minimum stress. *Precision Engineering*, doi:10.1016/j.precisioneng.2015.03.003, 2015.

[10] Freire Gómez J, Booker JD and Mellor PH. Stress optimization of leaf-spring crossed flexure pivots for an active Gurney flap mechanism. *Proc. SPIE 9433*, San Diego (USA), 943307, 2015.

[11] Gere JM and Timoshenko SP. *Mechanics of Materials*. 2nd edition, Brooks/Cole Engineering Division, 1984.

[12] Przemieniecki JS. *Theory of matrix structural analysis*, 1st edition, McGraw-Hill, 1968.

[13] Punmia BC, Kumar Jain A and Kumar Jain A. *Comprehensive R.C.C. designs*. 1st edition, Laxmi Publications, 2005.

[14] Siemens PLM Software, NX, Motion Analysis, <http://www.plm.automation.siemens.com/en_gb/products/nx/for-simulation/motion-analysis/index.shtml> (29 April 2015).

[15] MathWorks, Matlab, <http://www.mathworks.co.uk/products/matlab/> (29 April 2015).

[16] Dassault Systemes, Simulia, Abaqus < http://www.3ds.com/products-services/simulia/products/abaqus/> (29 April 2015).